Earthquakes and Structures, *Vol. 8, No. 4 (2015) 889-913*
DOI: http://dx.doi.org/10.12989/eas.2015.8.4.889

Vibration characteristics change of a base-isolated building with semi-active dampers before, during, and after the 2011 Great East Japan earthquake

Maki Dan*, Yuji Ishizawa, Sho Tanaka, Shuchi Nakahara, Shizuka Wakayama and Masayuki Kohiyama[a]

Graduate School of Science and Technology, Keio University,
3-14-1 Hiyoshi, Kohoku-ku, Yokohama, Kanagawa, Japan

(Received April 5, 2014, Revised October 10, 2014, Accepted October 11, 2014)

Abstract. Structural vibration characteristics of a semi-active base-isolated building were investigated using seismic observation records including those of the 2011 Great East Japan earthquake (Tohoku earthquake). Three different types of analyses were conducted. First, we investigated the long-term changes in the natural frequencies and damping factors by using an ARX model and confirmed that the natural frequency of the superstructure decreased slightly after the main shock of the Tohoku earthquake. Second, we investigated short-term changes in the natural frequencies and damping factors during the main shock by using the N4SID method and observed different transition characteristics between the first and second modes. In the second mode, in which the superstructure response is most significant, the natural frequency changed depending on the response amplitude. In addition, at the beginning of the ground motion, the identified first natural frequency was high possibly as a result of sliding friction. Third, we compared the natural frequencies and damping factors between the conditions of a properly functional semi-active control system and a nonfunctional system, by using the records of the aftershocks of the Tohoku earthquake. However, we could not detect major differences because the response was probably influenced by sliding friction, which had a more significant effect on damping characteristics than did the semi-active dampers.

Keywords: base isolation system; semi-active damper; system identification; 2011 Great East Japan earthquake; structural response

1. Introduction

Many approaches have been used for seismic response reduction, e.g., dampers, base-isolation bearings, and active and semi-active vibration control devices based on control engineering. Among these, combined systems of the base isolation system and semi-active controller have been used in Japan. Sosokan (*Sosokan*), a nine-story university building at Yagami Campus, Keio University, which was completed in 2000, has a semi-active base-isolation system (Yoshida 2001),

*Corresponding author, Research Assistant, E-mail: dan13.f.raven@gmail.com
[a]Associate Professor, E-mail: kohiyama@sd.keio.ac.jp

http://www.techno-press.org/?journal=eas&subpage=7 ISSN: 2092-7614 (Print), 2092-7622 (Online)

and Minamikan (South Building), a 16-story university building at Mita Campus, Keio University, which was completed in 2005, also employs the same type of seismic response reduction system (Nagashima 2011). In this paper, we focus on the vibration characteristics of Sosokan.

Sosokan has semi-active dampers to suppress seismic response. However, this control system was not in service because of maintenance work during the period of February 10 to March 13, 2011, which includes the day the 2011 Great East Japan earthquake (Tohoku earthquake) occurred; the building performed as a passively-controlled base-isolated system. When the main shock of the earthquake occurred on March 11, engineers were working on the base isolation layer to inspect the semi-active base-isolation system; fortunately, none were injured. Only slight damage was detected in some locations, such as a bridge between Sosokan and a neighboring reinforced concrete building; thus the response of the building appeared to be effectively reduced by the base-isolation system. It should be noted that no falling objects were reported in the building, whereas many falling objects were observed in buildings on the same campus.

In previous studies (e.g., Furukawa *et al.* 2005), system identification of dynamic properties was performed using seismic data, in which the dynamic properties of the system were appropriately identified using optimization techniques. For Sosokan, system identification was conducted using data collected during the Tohoku earthquake by well-known methods, such as ARX model and N4SID (Nakajima *et al.* 2012). Natural periods and damping factors of the system were identified, and the structural parameters for the analysis model, the stiffness and damping coefficients, were updated from those assumed in the structural design. In this study, parameters of the passive dampers in the base isolation layer were identified with a Kelvin-Voigt model. Then, using the updated model, the performance of the semi-active base-isolated system was analyzed on the basis of response simulation using the records of an aftershock occurring on April 7, 2011, as an input for ground motion. On that day, the semi-active control system was operating properly.

Dan and Kohiyama (2013) conducted identification of the dynamic properties of the system by using data collected during the Tohoku earthquake by a newly proposed identification method using optimization with a genetic algorithm and showed the performance of the semi-active controller could be improved by using the structural properties of the updated building model for the control parameters. In the design stage of Sosokan, the passive dampers in the base isolation layer were modeled with a Kelvin-Voigt model, but the model of the passive dampers was modified to a Maxwell model in the identification stage. The updated structural model was employed to improve the parameters of the semi-active controller, which uses a linear-quadratic-Gaussian controller. The performance of the semi-active base-isolated system was analyzed on the basis of time history response simulations by using the records of the aftershocks on April 7 and April 11, 2011, during which the semi-active control was operational. The updated structural parameters were shown to give more accurate estimations of the actual behavior of the system compared with the original parameters. Therefore, accurate parameters are crucial for good performance of seismic response control.

This study focuses on the long- and short-term changes in vibration characteristics of Sosokan. Because this building is equipped with seismic observation systems, it acquired a large number of seismic records, approximately 300, from May 2, 2006, to February 11, 2014. In this paper, three analyses and comparisons are conducted using these seismic records. First, we examined the changes of the natural frequencies and damping factors due to long-term changes by using the observed seismic records. Second, the changes in the natural frequencies and damping factors owing to the main shock of the Tohoku earthquake were investigated. Third, we compared the differences in the natural frequencies and damping factors between the conditions in which the

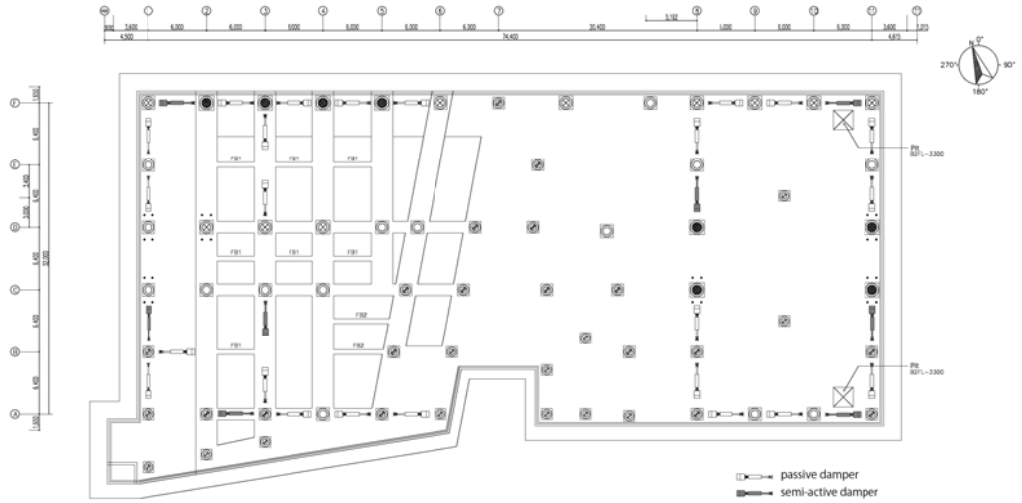

Fig. 1 Isolation layer plan of Sosokan

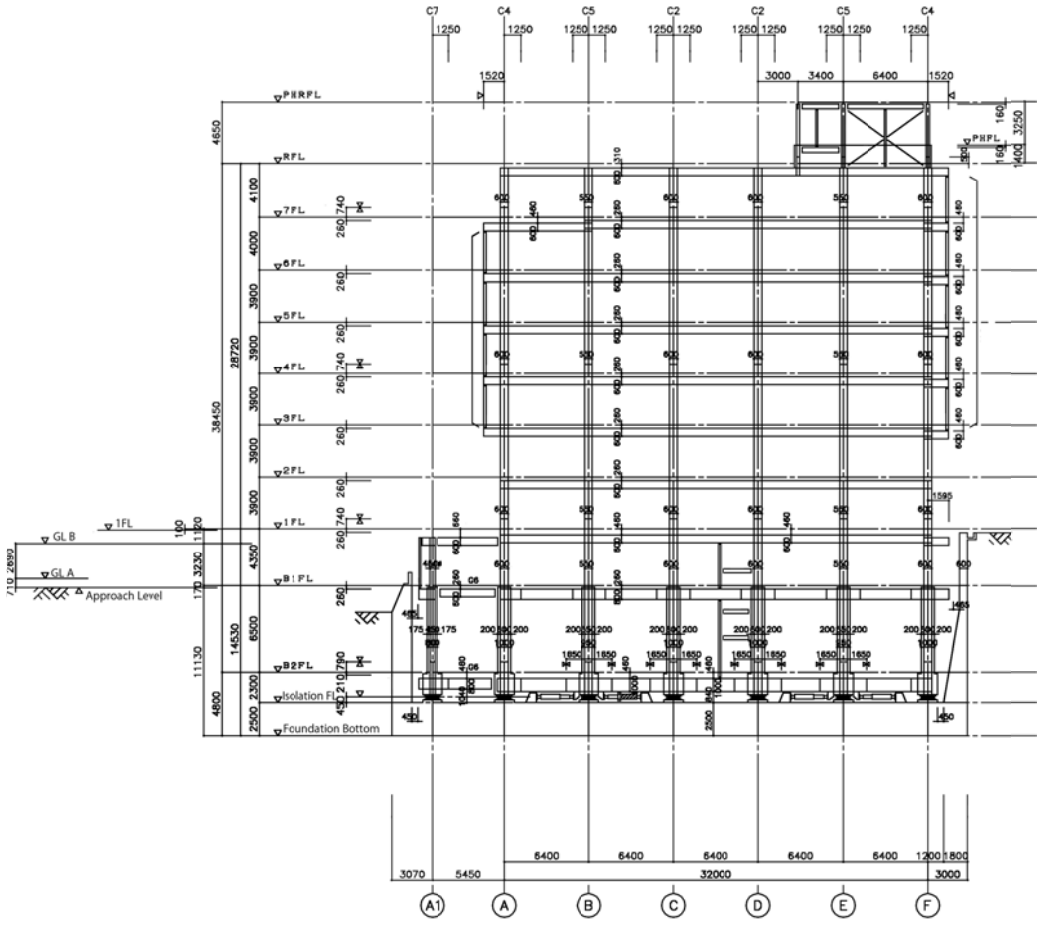

Fig. 2 Framing system of Sosokan

Table 1 Model parameters in the structural design

Floor	Mass [$\times 10^6$ kg]	Stiffness [$\times 10^6$ N/m]		Damping coefficient [$\times 10^6$ Ns/m]	
		NS direction	EW direction	NS direction	EW direction
RF	2.4999	1195.6	999.60	10.080	8.0487
7F	2.0664	1293.6	1156.4	10.906	9.3110
6F	2.0371	1499.4	1381.8	12.600	11.126
5F	2.0369	1577.8	1568.0	13.303	12.625
4F	2.0500	1715.0	1813.0	14.460	14.598
3F	2.0331	1724.8	1803.2	14.542	14.520
2F	1.8264	1773.8	1979.6	14.956	15.940
1F	2.4906	1979.6	2763.6	16.690	22.252
B1F	3.4382	1979.6	2273.6	16.690	18.306
B2F	4.9814	66.836	66.836	9.996	9.996
Base slab	—				

system was semi-actively and passively controlled. In this research, the natural frequencies and damping factors are identified using an ARX model (Mita 2003) and the N4SID method (Van Overschee and De Moor 1994) on the basis of the observation records.

2. Building properties

Fig. 1 shows Sosokan's isolation layer plan. The isolation layer is composed of 65 laminated natural rubber bearings, 24 passive hydraulic dampers, and eight semi-active dampers. The damping factor of the semi-active dampers can be switched among four settings. Fig. 2 shows the framing system of the building, which consists of steel, steel-reinforced concrete and concrete-filled steel tube members. The building has nine levels including seven floors above ground and two basement floors. The long axis of the building is oriented 25° to the south from the east direction, as shown in Fig. 1. For brevity, we refer to the short and long axes as North-South (hereafter, NS) and East-West (hereafter, EW) directions, respectively. The model parameters in the structural design are presented in Table 1.

Two independent seismic observation systems are installed in this building: one for controlling the semi-active system and one for research. In this study, we used the records collected by the latter system. In the latter system, accelerometers are placed at the foundation slab, the second basement floor (B2F), the first floor (1F), and the seventh floor (7F), as well as on the ground near the building. The former system has a displacement meter on the base-isolation layer but the latter one does not. Therefore, we integrated the acceleration records after applying a high-pass filterer to obtain displacements.

3. Long-term changes in structural vibration characteristics

The seismic observation system at Sosokan obtained 306 seismic records from May 2, 2006, to

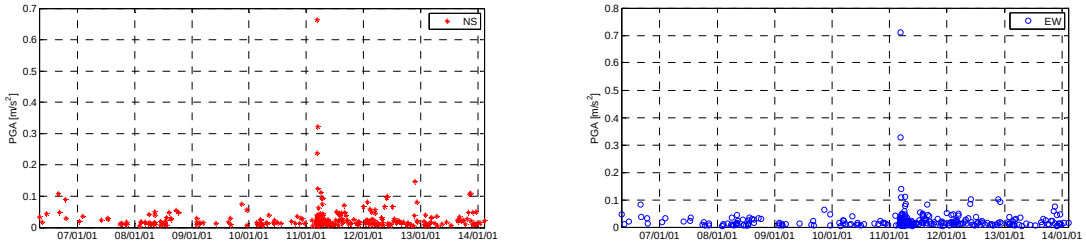

(a) NS direction (b) EW direction

Fig. 3 Peak ground acceleration distribution from October 24, 2010, to June 23, 2011

February 11, 2014 and their peak ground acceleration (hereafter, PGA) values are shown in Fig. 3. The maximum PGA was observed on March 11, 2011, which correlates with the main shock of the Tohoku earthquake. Numerous data were recorded soon after this main shock as aftershocks and induced earthquakes. As shown in Fig. 3, most of earthquake ground motions observed at Sosokan were smaller than 0.1 m/s^2.

Fig. 4 shows the natural frequencies and damping factors in the NS and EW directions, which were identified by using an ARX model. The acceleration records at the foundation slab were used as input, and those at 7F were used as output. With respect to the main shock of the Tohoku earthquake, the acceleration data between time 10 and 40 s, in which large amplitude of the principal shock was observed, were used for the estimation.

After the main shock of the Tohoku earthquake occurring on March 11, 2011, a slight decrease in the natural frequency of approximately 1 Hz, which corresponds to the natural frequency of the first mode of the superstructure above the isolation layer and the second mode of the entire building system, were confirmed by comparing the identified frequencies before the main shock. The average values of the natural frequencies at approximately 1 Hz before the main shock (records with PGA of ground motion smaller than 0.1 m/s) were 1.15 and 1.06 Hz in the NS and EW directions, respectively, and these changed to 1.06 and 0.995 Hz after the main shock in the NS and EW directions, respectively.

In the structural design, the first natural periods of the superstructure in the NS and EW directions were 1.32 and 1.27 s and those of the entire structure were 4.03 and 4.01 s, respectively. In addition, the damping ratio of the superstructure was 0.02 and that of the isolation device was 0.01 and 0.02 under the ground motions with peak ground velocity of 0.25 m/s and 0.50 m/s, respectively, in the structural design. The average values of the natural periods at approximately 1 s before the main shock (the reciprocals of the average natural frequencies) were 0.871 and 0.933 s in the NS and EW directions, respectively, and these changed to 0.941 and 1.01 s after the main shock in the NS and EW directions, respectively. This 7% elongation change is arguably attributed to the large superstructure response during the main shock, which could have caused loosening of the non-structural members and damage to the concrete parts of the structural members.

When the PGA was small, the identified natural periods of the first mode of the ARX model were approximately 1 s in almost all cases. On the contrary, when the PGA was large, the identified natural periods of the first mode tended to be much longer than 1 s. This difference may be due to the sliding friction in the isolation layer. Many non-structural members, such as equipment piping in the isolation layer and expansion joints between the building and the

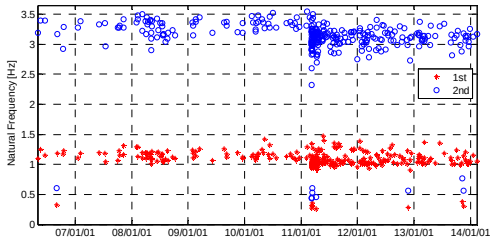

(a) Natural frequencies in the NS Direction

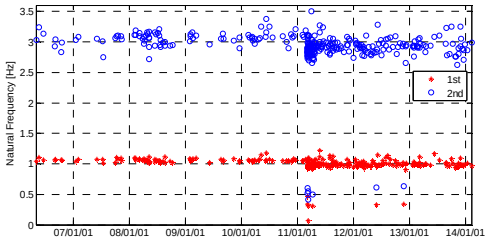

(b) Natural frequencies in the EW direction

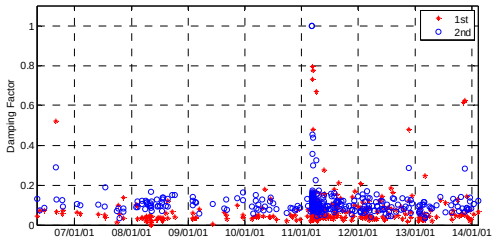

(c) Damping factors in the NS Direction

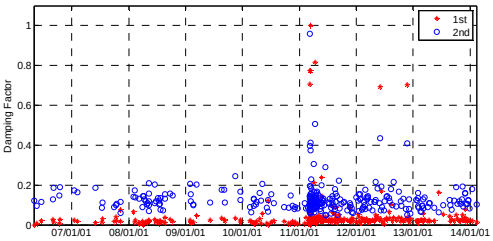

(d) Damping factors in the EW direction

Fig. 4 Vibration mode parameters identified by the ARX model

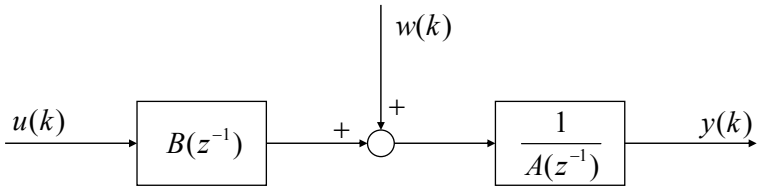

Fig. 5 A block diagram of an ARX model

surrounding moat wall, are adhered; thus, the isolation layer would not have deformed to the expected degree when the PGA was small. In this case, the superstructure response dominated, and the natural period of the base-isolation mode tended not to be identified.

For the damping factors, we could not obtain any remarkable results. Therefore, a different identification method, the N4SID method, was employed for subsequent investigation.

The block diagram of an ARX model for system identification is shown in Fig. 5, in which functions $A(z^{-1})$ and $B(z^{-1})$ satisfy the following equation

$$A(z^{-1})y(k) = B(z^{-1})u(k) + w(k) \tag{1}$$

where $u(k)$, $y(k)$, $w(k)$, and z^{-1} are the input, the output, the observation noise, and the delay operator, respectively. Assuming that the relationship between $u(k)$ and $y(k)$ can be formulated as Eq. (2), we can obtain the transfer function of the system $G(z^{-1})$ and the noise model $H(z^{-1})$ as (3) and (4), respectively.

$$y(k) = G(z^{-1})u(k) + H(z^{-1})w(k) \tag{2}$$

Table 2 The parameters used in the analysis of system identification

Parameter	Value
Number of poles, n_a	12
Number of zeroes plus 1, n_b	4
Number of dead time, n_k	1
Sampling frequency after decimation, $1/\Delta t$	3 Hz for the records with PGA greater than 0.1 m/s 30 Hz for other records

$$G(z^{-1}) = \frac{B(z^{-1})}{A(z^{-1})} \quad \text{and} \quad H(z^{-1}) = \frac{1}{A(z^{-1})} \tag{3),(4)}$$

Therefore, the pole of the transfer function p_i can be calculated as follows

$$G(z^{-1}) = \frac{B(z^{-1})}{A(z^{-1})} = k + \sum_{i=1}^{n_a} \frac{r_i}{1 - p_i z^{-1}}, \tag{5}$$

where n_a, k, and r_i are the number of poles, the constant, and the residue obtained by partial fraction decomposition, respectively. Using the i-th pole p_i, the natural frequency ω_i and the damping factor ζ_i can be estimated by the following equations, respectively

$$\omega_i = \frac{|\log p_i|}{\Delta t} = \frac{\sqrt{(\log|p_i|)^2 + (\arg|p_i|)^2}}{\Delta t} \quad \text{and} \quad \zeta_i = -\frac{\log|p_i|}{\omega_i \Delta t} \tag{6),(7)}$$

Note that Δt is the sampling time in the analysis of system identification, which is decided on the basis of the original first and second natural frequencies of the system. The parameters used in the system identification analysis are determined with reference to Adachi (2008) and Nakajima *et al.* (2012) and those values are listed in Table 2.

4. Short-term changes in structural vibration characteristics

When the main shock of the Tohoku earthquake occurred, the semi-active control system in Sosokan was turned off because of maintenance work. In this section, we analyze short-term changes in structural vibration characteristics that occur during an earthquake, such as natural frequencies and damping factors, by using records of the main shock of the Tohoku earthquake.

Figs. 6-8 show the time histories of ground acceleration (observed at the foundation slab), isolation layer drift, and relative displacement between B2F and 7F, respectively. The duration of the acquired record was 594 s (approximately 10 minutes), and the ground motion includes seismic waves of several aftershocks, as listed in Table 3 in the Appendix A.

Figs. 9 and 10 show the time histories of the changes in the natural frequencies and damping factors during the main shock, respectively, which were identified using the N4SID method. Details of the N4SID method are explained in the Appendix B. In the system identification, numerical integration was first carried out to obtain displacement data from the acceleration records after applying a third-order Butterworth high-pass causal filter with a cutting frequency of

0.125 Hz. Then, the displacement data were cropped by a time window of 40 s and the starting time of the window was moved with the time interval of 5 s.

As shown in Fig. 9, the natural frequencies have high values in the initial part of the time history due to the behavior of the adhered isolation layer. After the isolation layer began to deform largely after the time instant 100 s, the natural frequencies became stable. The natural frequency of the first mode was maintained at approximately 0.3 Hz until the end of the records. The natural frequency of the second mode became smaller as the relative displacement between B2F and 7F increased, which appeared to be dependent on the superstructure response magnitude.

In Fig. 10, the damping factors of the first mode appear to be influenced by sliding friction in the isolation layer. Therefore, its average value and fluctuation are larger than those of the second mode. The coefficient of variation of the first damping factor is about 3% larger than the second damping factor in the NS direction, and about 8% larger in the EW direction.

Fig. 11 shows the transition of the power spectrum density (PSD) during the main shock. As shown in Figs. 6-8, ground acceleration was large between 100 and 150 s. In addition, the PSD was large between 0 Hz and 3 Hz during this period, and both the first and second modes were excited. The natural frequency of the first mode was approximately 0.3 Hz and the PSD at the frequency of 0.3 Hz remained large until 400 s. The first mode vibration remained excited; therefore, the natural frequency of the first mode remained stable, as shown in Fig. 9.

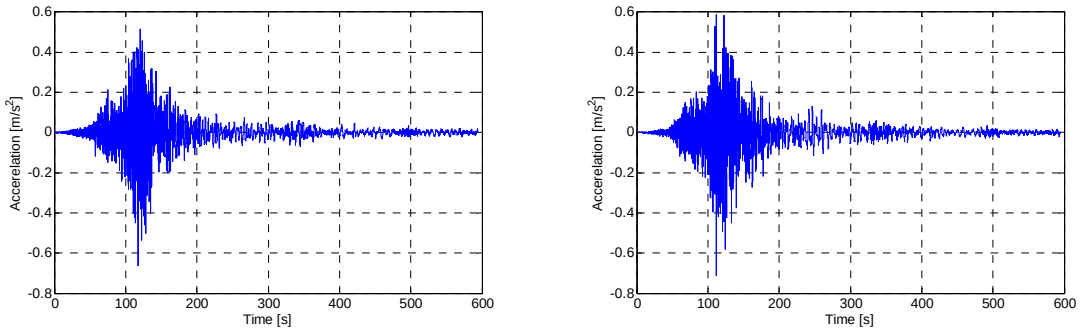

(a) NS direction (b) EW direction

Fig. 6 Time histories of ground acceleration during the main shock of the Tohoku earthquake

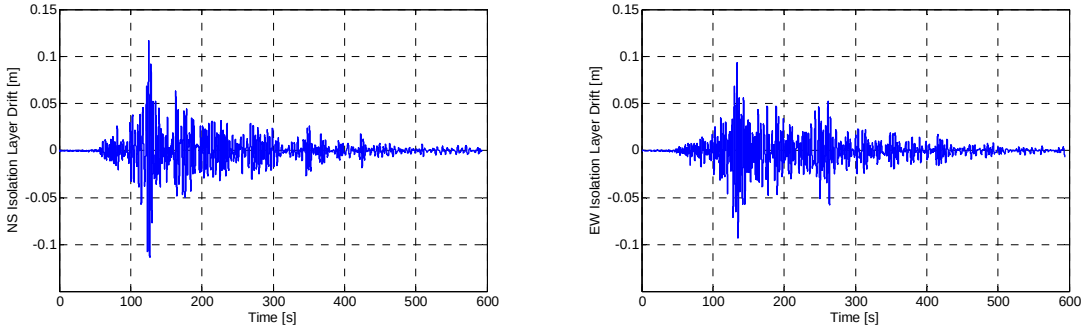

(a) NS direction (b) EW direction

Fig. 7 Time histories of isolation layer drift during the main shock of the Tohoku earthquake

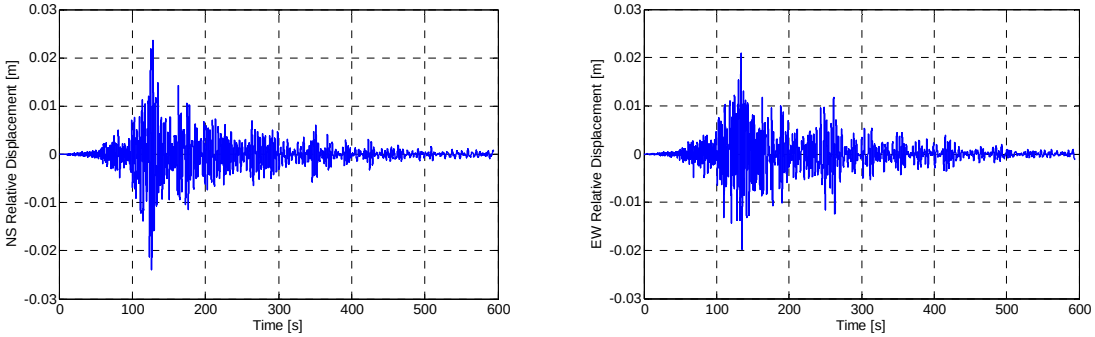

(a) NS direction (b) EW direction

Fig. 8 Time histories of relative displacement between B2F and 7F during the main shock of the Tohoku earthquake

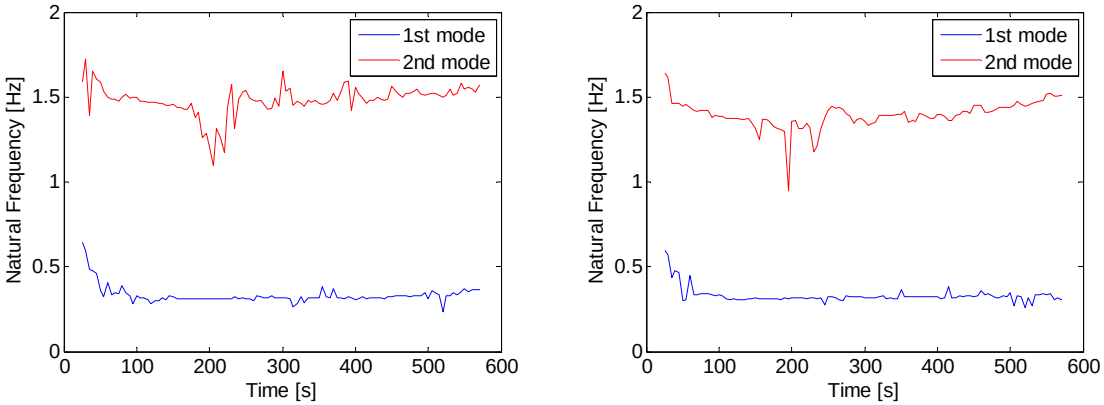

(a) NS direction (b) EW direction

Fig. 9 Transition of natural frequencies during the main shock of the Tohoku earthquake

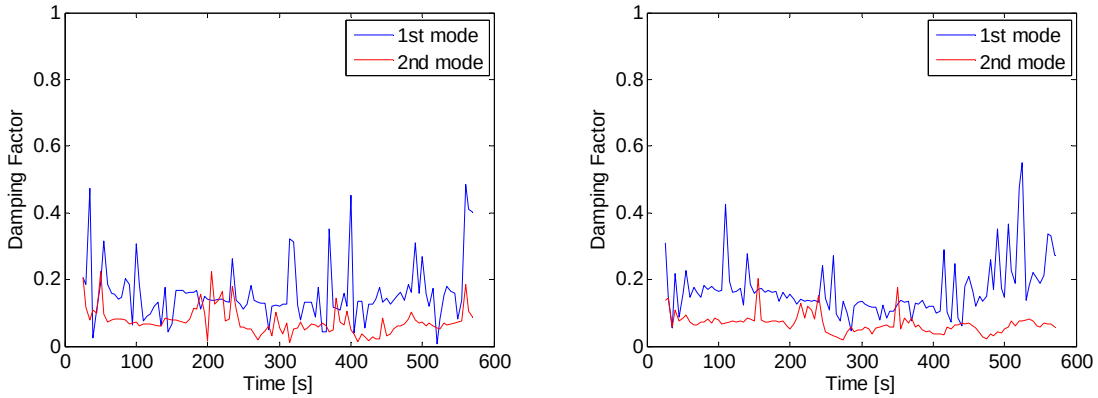

(a) NS direction (b) EW direction

Fig. 10 Transition of damping factors during the main shock of the Tohoku earthquake

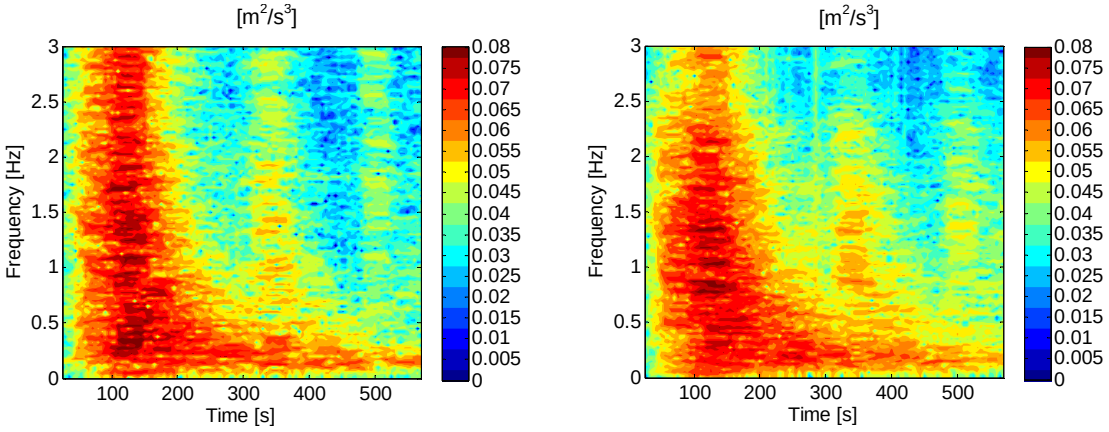

(a) NS direction (b) EW direction

Fig. 11 Transition of PSD during the main shock of the Tohoku earthquake

5. Difference of structural vibration characteristics between the control conditions

The semi-active control system in Sosokan was not in service because of maintenance work from February 10 to March 13, 2011. In this section, structural vibration characteristics are compared between semi-actively-controlled and passively-controlled systems. As mentioned before, Sosokan has passive hydraulic dampers and semi-active dampers. Hereafter, we refer to the condition that the semi-active dampers operated properly as *the semi-actively controlled system* and the condition that they did not operate and behaved like passive dampers as *the passively controlled system*. The two different records are used for both semi-actively and passively controlled systems in the analysis to effectively observe the characteristics of each controlled system. The information of earthquakes related to the records is presented in Tables 3 and 4 in

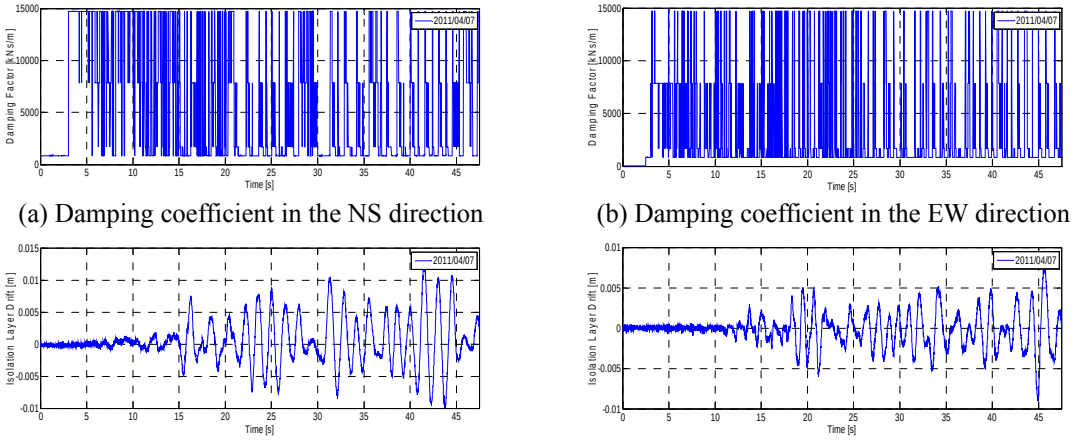

(a) Damping coefficient in the NS direction (b) Damping coefficient in the EW direction

(c) Isolation layer drift in the NS direction (d) Isolation layer drift in the EW direction

Fig. 12 Switched damping coefficient of a semi-active damper and isolation layer drift in the April 7, 2011 record

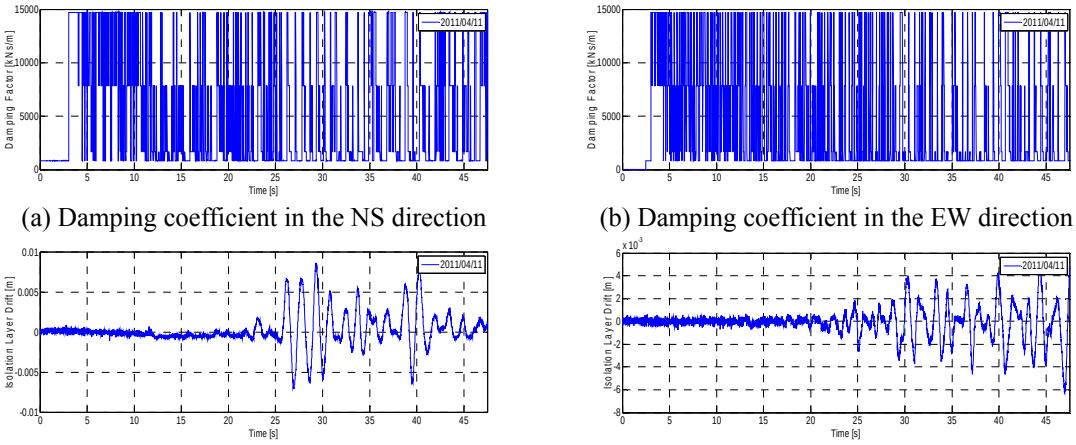

(a) Damping coefficient in the NS direction (b) Damping coefficient in the EW direction

(c) Isolation layer drift in the NS direction (d) Isolation layer drift in the EW direction

Fig. 13 Switched damping coefficient of a semi-active damper and isolation layer drift in the April 11, 2011 record

Appendix A and the switched damping coefficients of a semi-active damper are shown in Figs. 12 and 13, which were collected by the observation system for the semi-active controller. The damping ratios became larger than that using the minimum value of the switched damping coefficients.

Figs. 12 and 13 show the damping coefficient change of a single semi-active damper, which was calculated from a control signal recorded by the observation system for the semi-active controller. There are four semi-active dampers in each direction. The isolation layer displacements measured by a displacement meter are also shown in the figures.

5.1 Results of the semi-actively controlled system

Figs. 14-16 respectively show the time histories of ground acceleration, isolation layer drift, and relative displacement between B2F and 7F derived from the records observed at 23:34 on

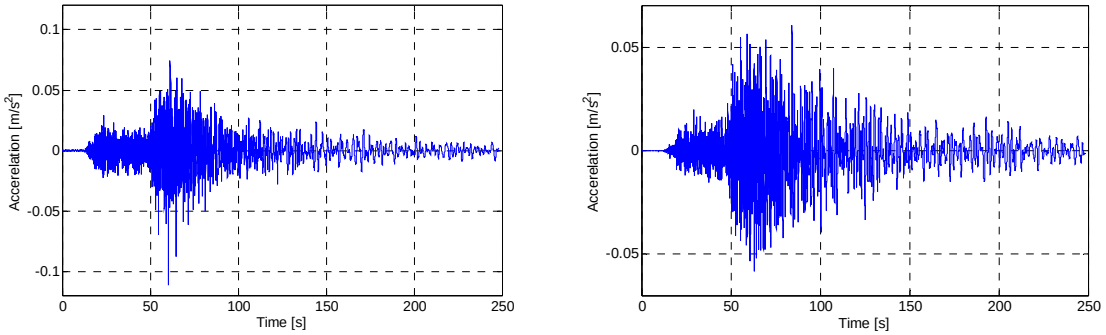

(a) NS direction (b) EW direction

Fig. 14 Time histories of the ground acceleration (record: 23:34 on April 7, 2011)

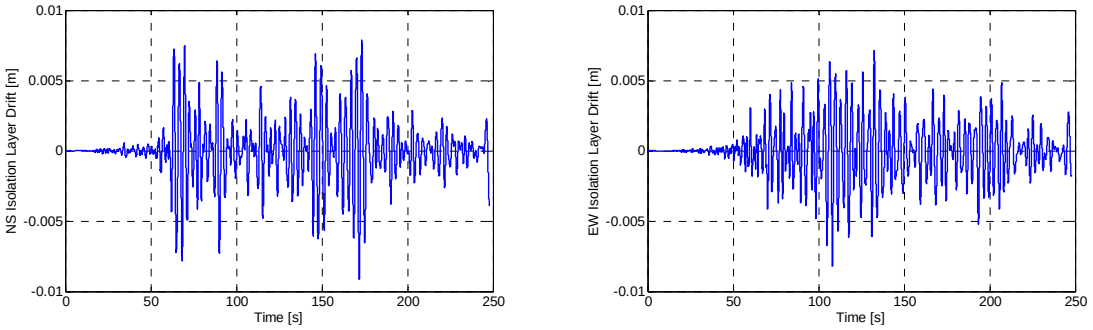

(a) NS direction (b) EW direction

Fig. 15 Time histories of isolation layer drift (record: 23:34 on April 7, 2011)

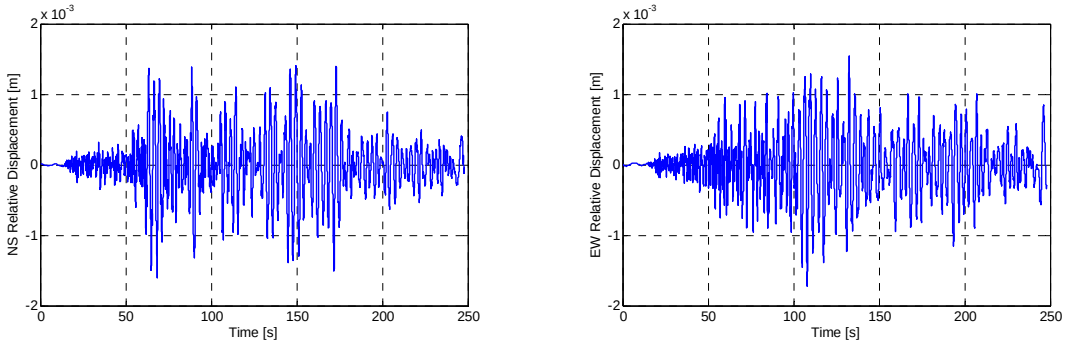

(a) NS direction (b) EW direction

Fig. 16 Time histories of relative displacement between B2F and 7F (record: 23:34 on April 7, 2011)

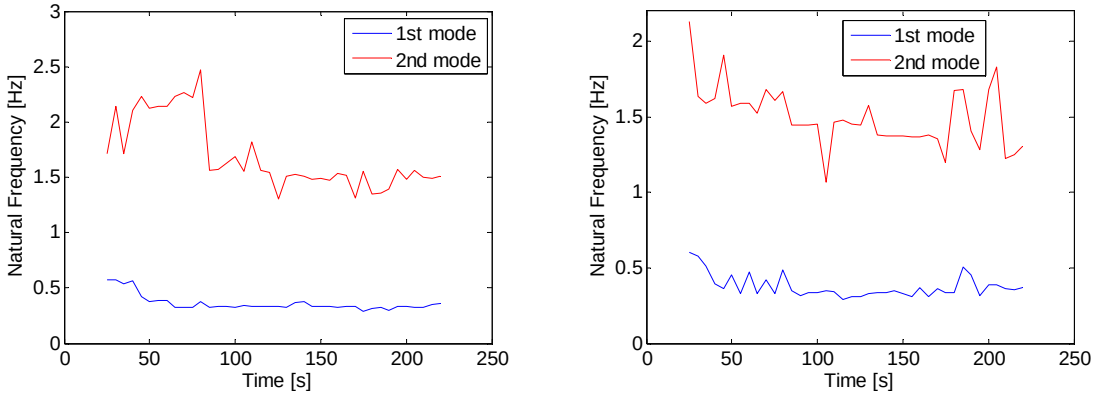

(a) NS direction (b) EW direction

Fig. 17 Transition of natural frequencies (record: 23:34 on April 7, 2011)

April 7, 2011. Figs. 17 and 18 show the transition of natural frequencies and damping factors, respectively. Fig. 19 shows the transition of the PSD in ground acceleration.

Figs. 20-22 show the time histories of the ground acceleration, isolation layer drift, and relative displacement between B2F and 7F in the record observed at 17:17 on April 11, 2011, respectively. Figs. 23 and 24 show the transition of the natural frequencies and damping factors, respectively. Fig. 25 shows the transition of the PSD.

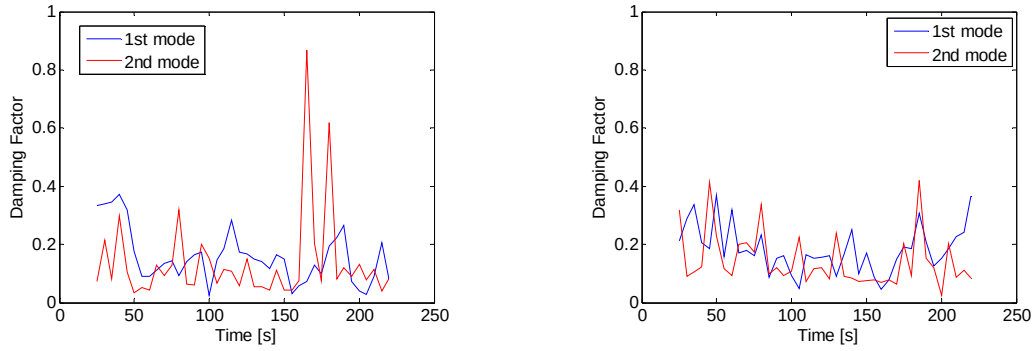

(a) NS direction (b) EW direction

Fig. 18 Transition of damping factors (record: 23:34 on April 7, 2011)

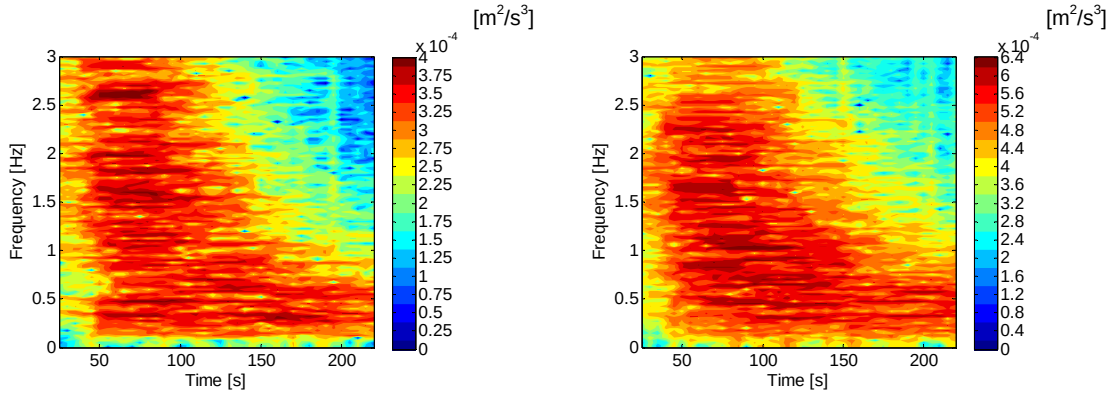

(a) NS direction (b) EW direction

Fig. 19 Transition of PSD (record: 23:34 on April 7, 2011)

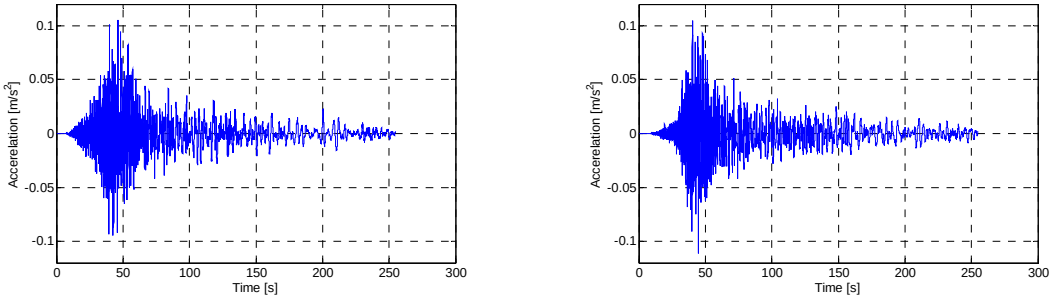

(a) NS direction (b) EW direction

Fig. 20 Time histories of ground acceleration (record: 17:17 on April 11, 2011)

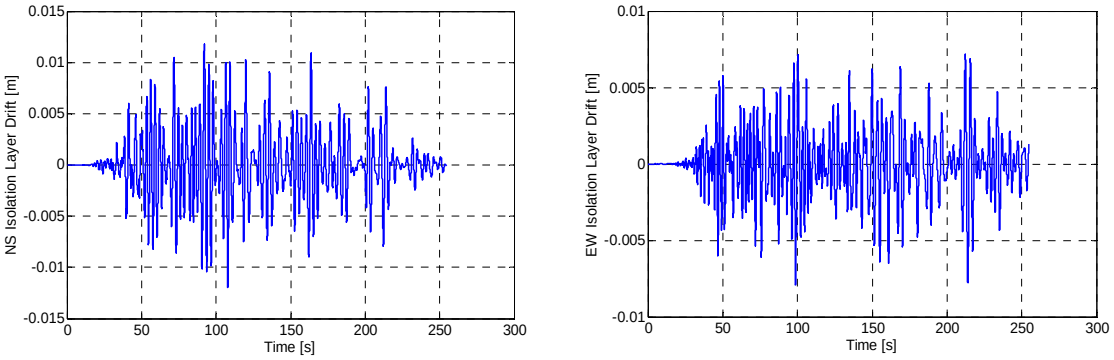

(a) NS direction (b) EW direction

Fig. 21 Time histories of isolation layer drift (record: 17:17 on April 11, 2011)

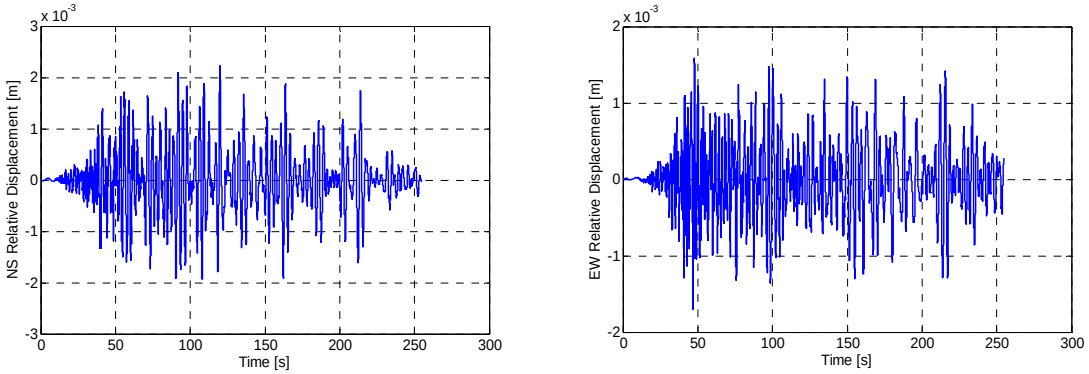

(a) NS direction (b) EW direction

Fig. 22 Time histories of relative displacement between B2F and 7F (record: 17:17 on April 11, 2011)

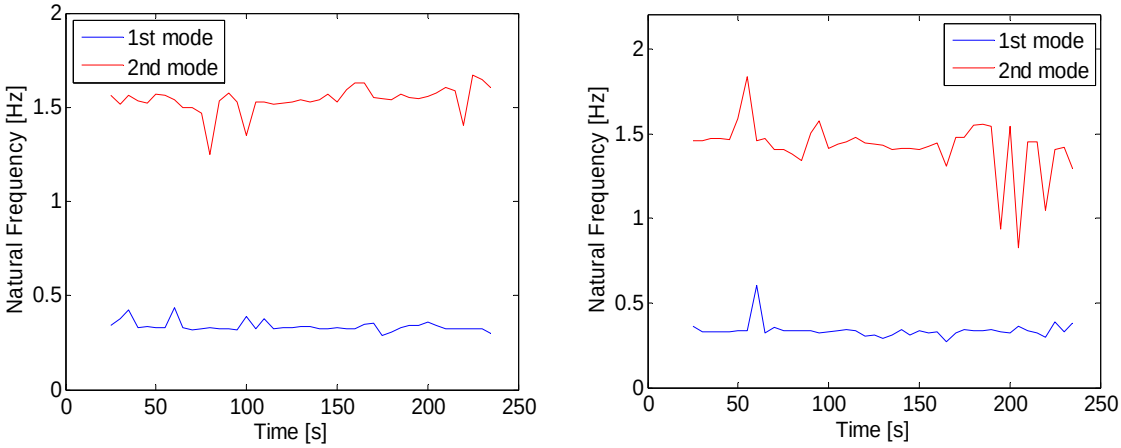

(a) NS direction (b) EW direction

Fig. 23 Transition of natural frequencies (record: 17:17 on April 11, 2011)

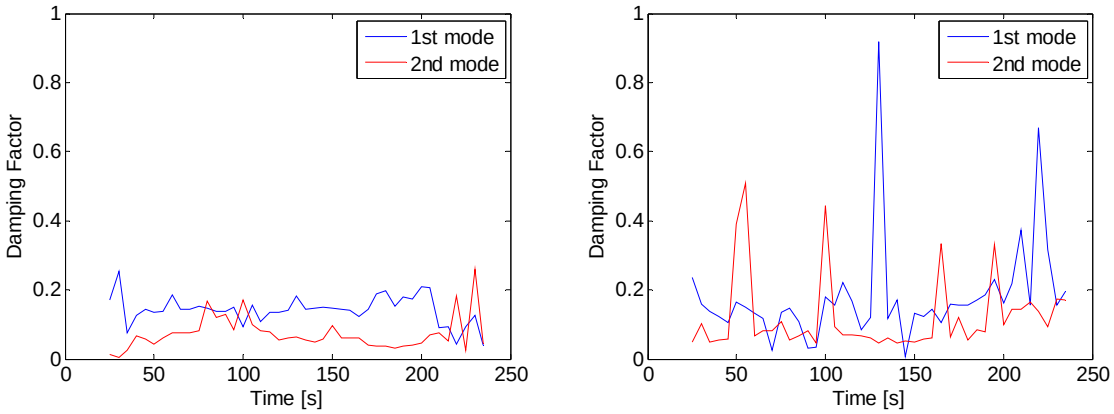

(a) NS direction (b) EW direction

Fig. 24 Transition of damping factors (record: 17:17 on April 11, 2011)

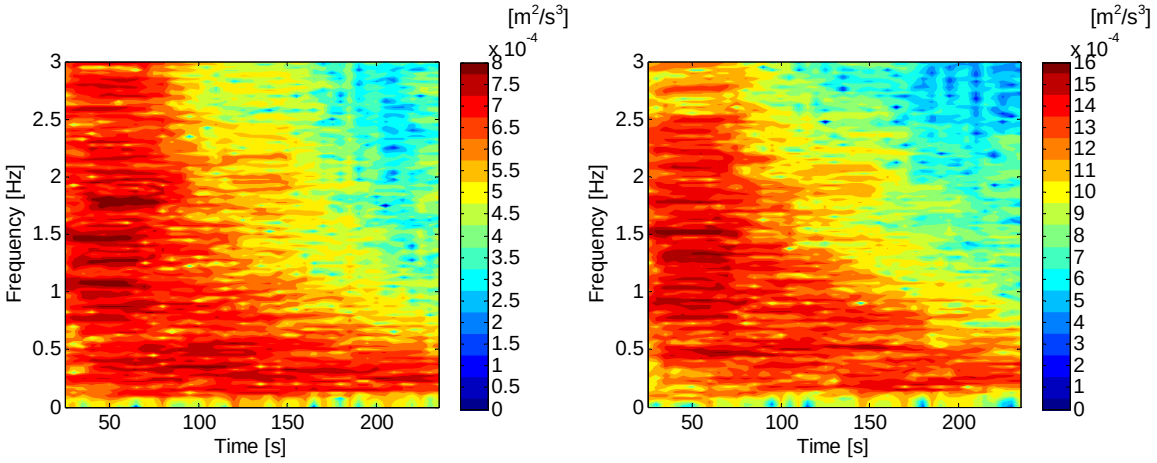

(a) NS direction (b) EW direction

Fig. 25 Transition of PSD (record: 17:17 on April 11, 2011)

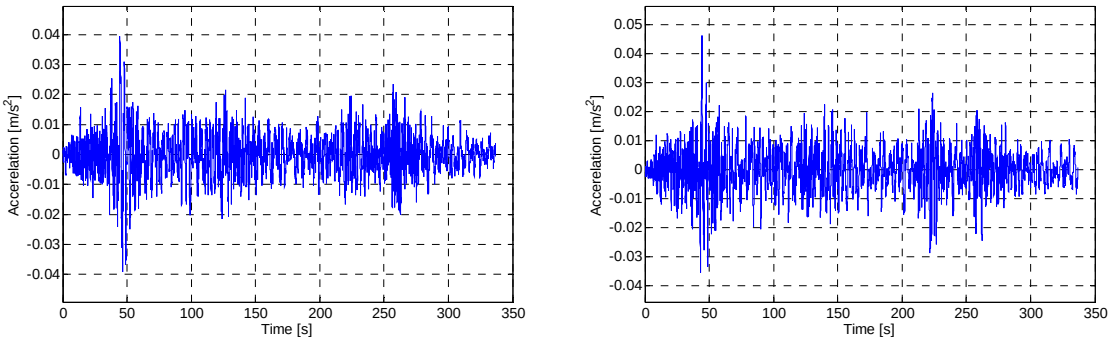

(a) NS direction (b) EW direction

Fig. 26 Time histories of the ground acceleration (record: 15:08 on March 11, 2011)

5.2 Results of passively-controlled system

Figs. 26-28 respectively show the time histories of ground acceleration, isolation layer drift, and relative displacement between B2F and 7F in the record observed at 15:08 on March 11, 2011. Figs. 29 and 30 show the transition of natural frequencies and damping factors, respectively. These figures show large scatter because the intensity of the input is small. Fig. 31 shows the transition of the PSD.

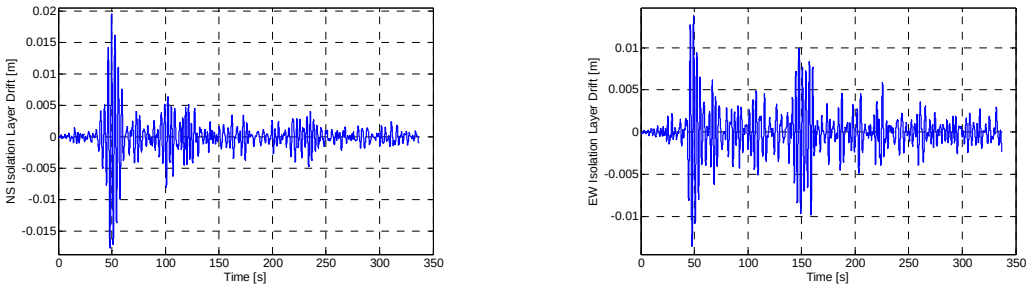

(a) NS direction (b) EW direction

Fig. 27 Time histories of isolation layer drift (record: 15:08 on March 11, 2011)

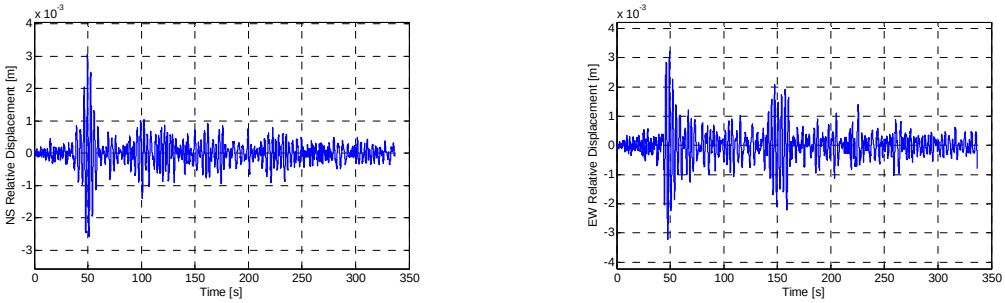

(a) NS direction (b) EW direction

Fig. 28 Time histories of relative displacement between B2F and 7F (record: 15:08 on March 11, 2011)

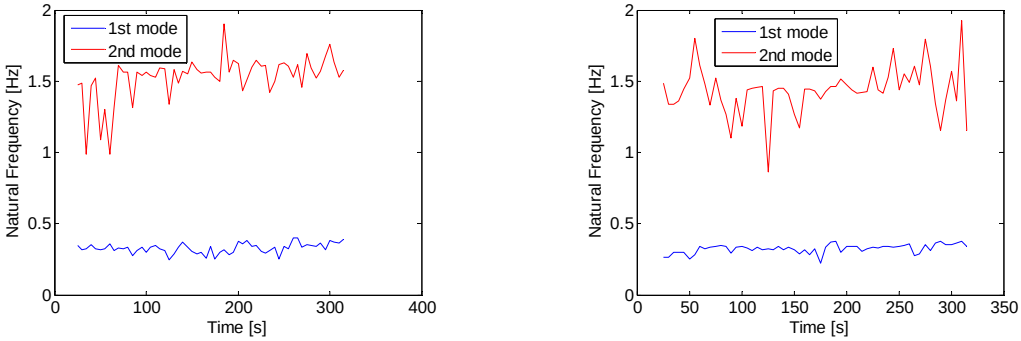

(a) NS direction (b) EW direction

Fig. 29 Transition of natural frequencies (record: 15:08 on March 11, 2011)

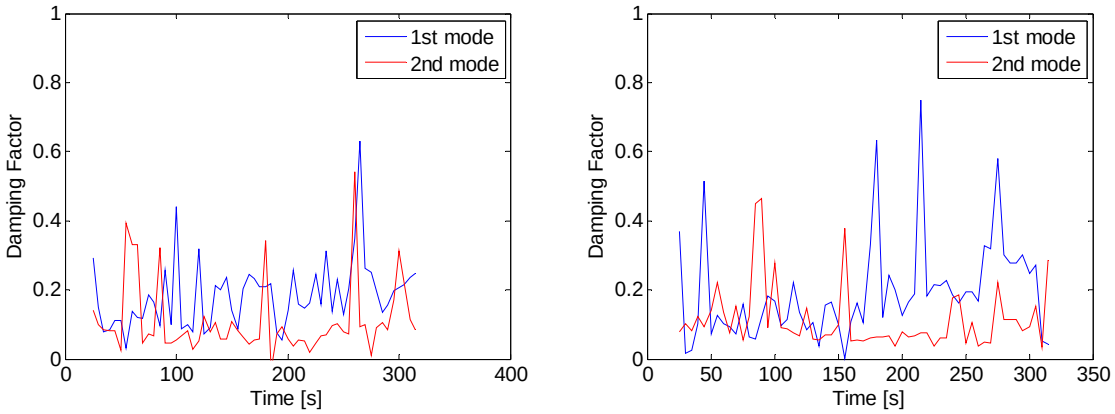

(a) NS direction (b) EW direction

Fig. 30 Transition of damping factors (record: 15:08 on March 11, 2011)

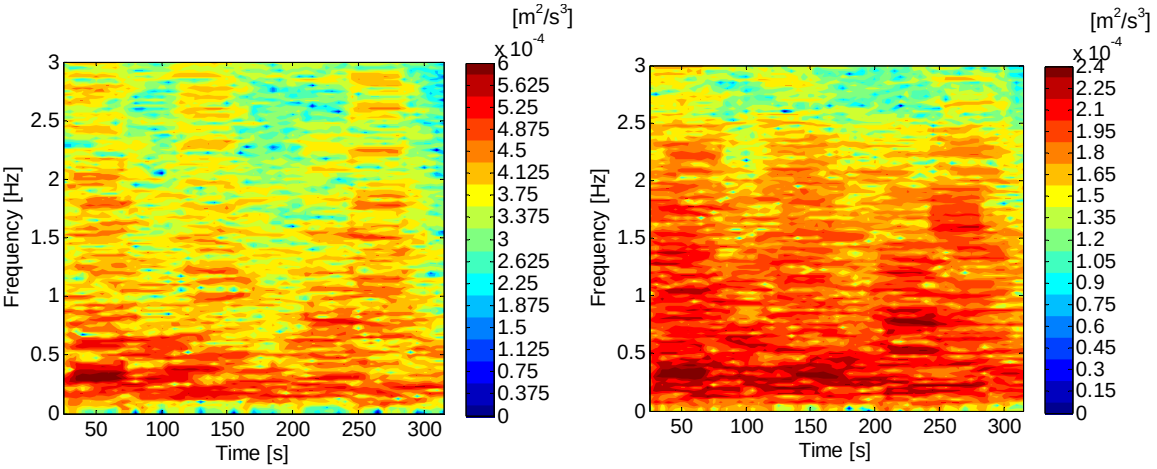

(a) NS direction (b) EW direction

Fig. 31 Transition of PSD (record: 15:08 on March 11, 2011)

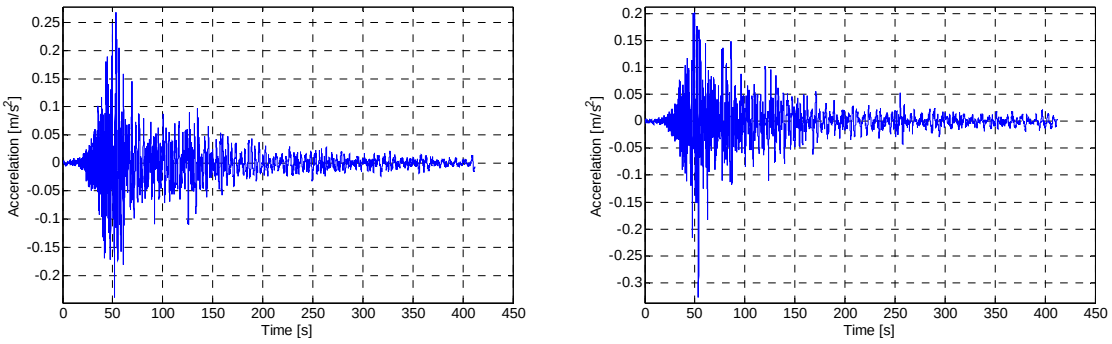

(a) NS direction (b) EW direction

Fig. 32 Time histories of ground acceleration (record: 15:16 on March 11, 2011)

Figs. 32-34 respectively show the time histories of ground acceleration, isolation layer drift, and relative displacement between B2F and 7F of the record observed at 15:16 on March 11, 2011. Figs. 35 and 36 show the transition of natural frequencies and damping factors, respectively. In the same manner with Figs. 29 and 30, Figs. 35 and 36 show large scatter because the intensity of the input is small. Fig. 37 shows the transition of the PSD.

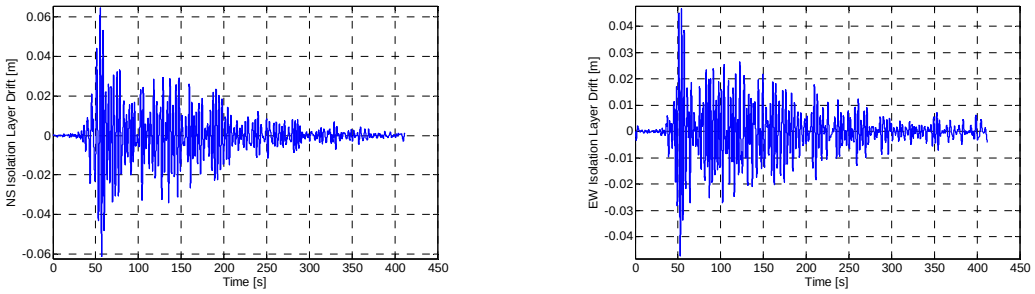

(a) NS direction (b) EW direction

Fig. 33 Time histories of isolation layer drift (record: 15:16 on March 11, 2011)

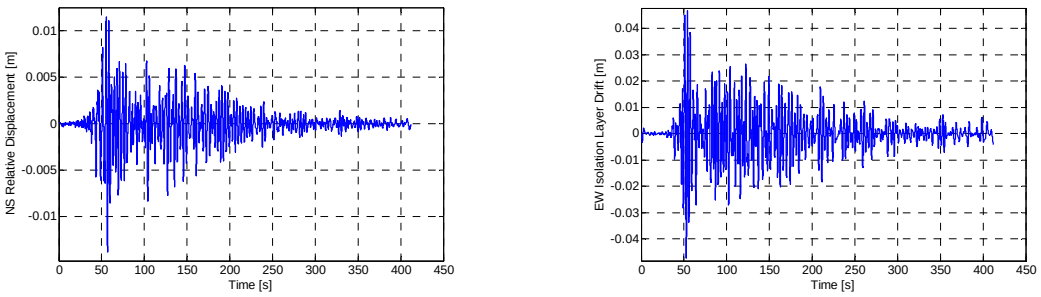

(a) NS direction (b) EW direction

Fig. 34 Time histories of relative displacement between B2F and 7F (record: 15:16 on March 11, 2011)

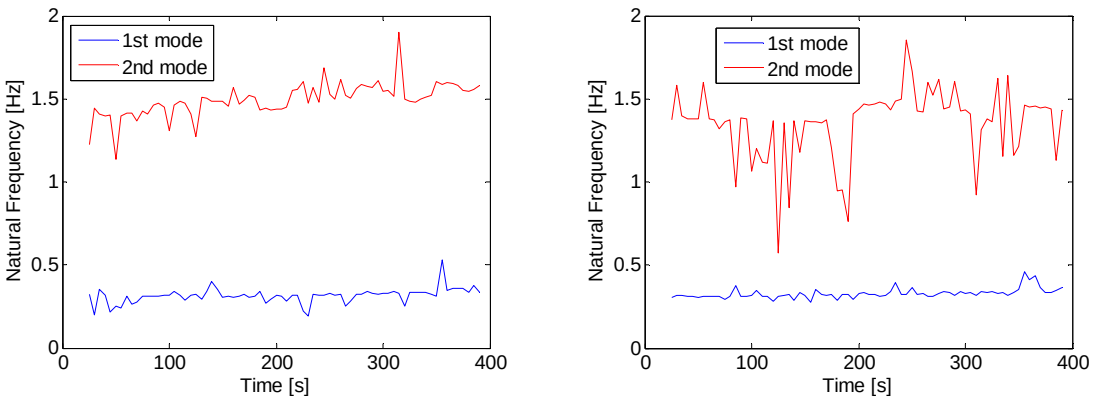

(a) NS direction (b) EW direction

Fig. 35 Transition of natural frequencies (record: 15:16 on March 11, 2011)

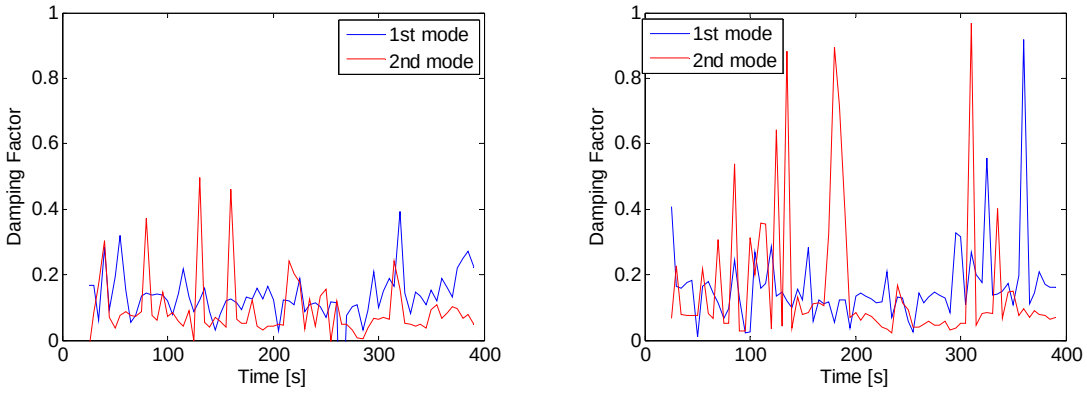

(a) NS direction (b) EW direction

Fig. 36 Transition of damping factors (record: 15:16 on March 11, 2011)

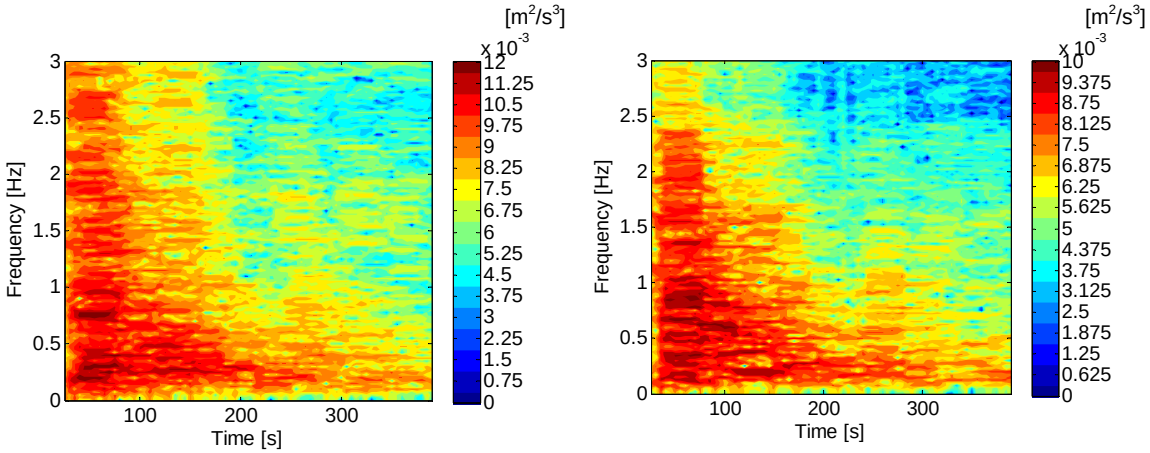

(a) NS direction (b) EW direction

Fig. 37 Transition of PSD (record: 15:16 on March 11, 2011)

5.3 Comparative studies

The first natural frequencies of both semi-actively and passively controlled systems were approximately 0.3 Hz and they appeared to be stable. It can be considered that the seismic isolation bearing made of natural rubber has relatively constant stiffness regardless of its deformation amplitude. The natural frequency of the second mode appeared to change largely, however this is attributed to the record length difference and there were less differences in comparing the unit time change.

As for the damping factors, it was hard to detect visible differences between the semi-actively and passively controlled systems. As shown in the above figures, the damping factors were not stable compared with the natural frequencies. The sliding friction would influence to those instabilities. The damping factors of the second mode tended to be smaller than that of the first mode. The damping factor of the first mode were increased by the oil dampers set on the base

isolation layer. However, in the second mode, the superstructure response was most significant and the damping factors of the second mode were less influenced by the oil dampers.

The earthquake ground motions in the record used in this comparative analysis were those of the aftershocks of the Tohoku earthquake. Several differences were observed in the transition of PSD between the main shock and aftershocks. The PSD of the main shock in Fig. 11 included long-period components. Sosokan is located on the Kanto sedimentary basin so that long-period waves tend to keep reflecting in the sediment layer. However, this phenomenon could not be observed in the aftershocks records in Figs. 19, 25, 31, and 37 because the magnitudes of the aftershocks were relatively small and log-period waves were not emitted.

6. Conclusions

This study conducted three different types of analysis by using seismic records acquired in a university building with a semi-active base-isolation system. First, we investigated the long-term changes in the natural frequencies and damping factors during a seven-year-and-nine-month period including the occurrence date of the 2011 Tohoku earthquake. An ARX model was employed in the system identification. Second, the short-term changes in the natural frequencies and damping factors during the main shock of the Tohoku earthquake were investigated, in which we employed the N4SID method and moving time windows in the system identification. Third, we conducted comparative studies to examine the difference in the vibration characteristics between conditions of a properly operating semi-active-controlled system and that not in operation. The records of the aftershocks of the Tohoku earthquake were used in the analysis.

In the long-term change analysis, a slight decrease in the natural frequency of approximately around 1 Hz was confirmed, which corresponds to the first mode of the superstructure, after the main shock of the Tohoku earthquake. However, it was difficult to detect differences in the damping factors, possibly because of the limitation of the employed method. In the short-term change analysis, the second mode, in which the superstructure showed the most significant response, appeared to have amplitude dependency. However, the first mode, in which the isolation layer was largely deformed, maintained a constant natural frequency value once the isolation layer experienced large deformation and appeared to have less amplitude dependency. In the comparative study between the passively and semi-actively controlled systems, we could not detect major differences in damping characteristics, which is likely due to the influence of sliding friction in the base isolation layer and because the semi-active oil dampers were less affected in the records used in the analysis. In addition, structural responses were smaller than those in the main shock records. Therefore, we conclude that large response records are necessary to comprehend the characteristics of the semi-active base-isolated system and to inspect its performance under strong ground motion.

Acknowledgments

This research was supported by a JSPS KAKENHI Grant-in-Aid for Scientific Research (B), Grant Number 24360230.

References

Adachi, S. (2014), "Performance evaluation of system identification in frequency domain", *J. Soc. Instrument Control Eng.*, **47**(11), 915-920. (in Japanese)

Adachi, S. (2004), *MATLAB ni yoru Seigyo no tameno Jōkyū Shisutemu Dōtei (Advanced System Identification for Control Using MATLAB)*, Tokyo Denki University Press, Tokyo, Japan. (in Japanese)

Association for Development of Earthquake Prediction (2014), *Jishin Kasokudo Jōhō (Information of Seismic Acceleration)*, http://www.adep.or.jp/kanren/kasokudo.html

Dan, M. and Kohiyama, M. (2013), "System identification and control improvement of a semi-active-controlled base-isolated building using the records of the 2011 Great East Japan Earthquakes", *Proceedings of the 11th International Conference on Structural Safety and Reliability*, New York, USA.

Furukawa, T., Ito, M., Izawa, K. and Noori, M. (2005), "System identification of base-isolated building using seismic response data", *J. Eng. Mech.*, **131**(3), 268-275.

Ljung, L. (1999), *System Identification: Theory for the User*, 2nd edition, Prentice-hall, Upper Saddle River, New Jersey, USA.

Mita, A. (2003), *Structural dynamics for health monitoring*, Sankeisha Co., Ltd, Nagoya, Japan, 114.

Nagashima, I., Maseki, R., Shinozaki, Y., Yoyama, J. and Kohiyama, M. (2011), "Study on performance of semi-active base-isolation system using earthquake observation records," *Proceedings of the International Symposium on Disaster Simulation and Structural Safety in the Next Generation*, Kobe, Japan.

Nakajima, K., Giron, N., Kohiyama, M., Watanabe, K., Yoshida, M., Yamanaka, M., Inaba, S., and Yoshida, O. (2012), "Seismic response analysis of a semi-active-controlled base-isolated building during the 2011 Great East Japan Earthquake", *Proceedings of the International Symposium on Engineering Lessons Learned from the Giant Earthquake*, Tokyo, Japan.

Van Overschee, P. and De Moor, B. (1994), "N4SID: Subspace Algorithms for the Identification of Combined Deterministic-Stochastic Systems", *Automatica*, **30**(1), 75-93.

Yoshida, K. (2001), "First building with semi-active base isolation", *J. Japan Soc. Mech. Eng.*, **104**(995), 698-702. (in Japanese)

CN

Appendix A: The information of earthquakes related to the records

The earthquake properties related to the observation records used in this study are shown in Tables 3 and 4. These properties are cited from the Web inquiry system of the Association for Development of Earthquake Prediction, which uses data from the meteorological data switching system of Japan Meteorological Agency (JMA). Sosokan is located at latitude 35.5554°N and longitude 139.6537°E.

Table 3 Earthquake properties for records in the case in which the system is passively controlled

Time of occurrence (Year/Month/Day Time)	Epicenter region	Magnitude	Epicenter	Focal depth [km]	JMA seismic intensity at eastern Kanagawa
The main shock of the Tohoku earthquake on March 11, 2011					
2011/03/11 14:46:18	Sanriku-oki	9.0	38.1°N, 142.9°E	24	5+
Aftershocks and induced earthquakes of the Tohoku earthquake on March 11, 2011					
2011/03/11 14:51:20	Fukushima-ken-oki	6.8	36.7°N, 142.0°E	33	3
2011/03/11 14:54:31		6.1	37.5°N, 141.3°E	34	2
2011/03/11 15:06:10	Iwate-ken-oki	6.5	39.0°N, 142.4°E	29	2
2011/03/11 15:07:16	Ibaraki-ken-oki	6.5	36.3°N, 142.2°E	20	2
2011/03/11 15:08:20	Shizuoka-ken Izu area	4.6	35.2°N, 139.0°E	6	3
2011/03/11 15:08:53	Iwate-ken-oki	7.4	39.8°N, 142.8°E	32	3
2011/03/11 15:11:19	Northern Ibaraki-ken	5.5	36.9°N, 140.6°E	6	2
2011/03/11 15:15:34	Ibaraki-ken-oki	7.6	36.1°N, 141.3°E	43	5−
2011/03/11 15:18:12		4.7	36.0°N, 141.0°E	41	3
2011/03/11 15:19:03		5.7	36.3°N, 141.1°E	33	2
2011/03/11 15:20:01		5.8	36.1°N, 141.8°E	34	3
2011/03/11 15:20:44		5.7	36.6°N, 141.7°E	62	2

Table 4 Earthquake properties for records in the case in which the system is semi-actively controlled

Time of occurrence (Year/Month/Day Time)	Epicenter region	Magnitude	Epicenter	Focal depth [km]	JMA seismic intensity at eastern Kanagawa
Aftershock of the Tohoku earthquake on April 7, 2011					
2011/04/07 23:32:43	Miyagi-ken-oki	7.2	38.2°N, 141.9°E	66	3
Aftershock of the Tohoku earthquake on April 11, 2011					
2011/04/11 17:16:12	Fukushima-ken Hama-dori	7.0	37.0°N, 140.7°E	6	4
2011/04/11 17:19:31		4.5	37.0°N, 140.7°E	11	2
2011/04/11 17:20:26		4.2	37.0°N, 140.8°E	7	—

Appendix B: N4SID system identification procedure (Van Overschee and De Moor 1994, Ljung 1999, Adachi 2004)

N4SID (Numerical algorithms for Subspace State Space System Identification method) is one of the subspace methods available, which identifies state space models using input-output data. The N4SID method can obtain building models without non-linear optimization. These algorithms are stable, and have demonstrated a prominent accuracy of calculation. Including random excitation, *m*-input *p*-output linear discrete-time system is described as Eq. (B1).

$$\begin{cases} x(k+1) = Ax(k) + Bu(k) + w(k) \\ y(k) = Cx(k) + Du(k) + v(k) \end{cases} \tag{B1}$$

Here, $u(k) \in R^m$ is the input signal, $y(k) \in R^p$ is the output signal, $x(k) \in R^n$ is the state variable, $w(k) \in R^n$ is the system noise, and $v(k) \in R^p$ is the observed noise. To determine A, B, C, and D, we must estimate some variables. From Eq. (B1), $y(k+l)$ is transformed as follows

$$\begin{aligned} y(k+l) &= Cx(k+l) + Du(k+l) + v(k+l) \\ &= CAx(k+l-1) + CBu(k+l-1) + Cw(k+l-1) + Du(k+l) + v(k+l) \\ &\vdots \\ &= CA^l x(k) + CA^{l-1}Bu(k) + CA^{l-2}Bu(k+1) + \cdots + CBu(k+l-1) + Du(k+l) \\ &\quad + CA^{l-1}w(k) + CA^{l-2}w(k+1) + \cdots + Cw(k+l-1) + v(k+l) \end{aligned} \tag{B2}$$

With l being equal to 0 to $r-1$, the elements of Eq. (B2) are described according to Eqs. (B3)-(B5).

$$Y_r(k) = \begin{bmatrix} y(k) \\ y(k+1) \\ \vdots \\ y(k+r-1) \end{bmatrix} \in R^{pr\times 1}, \quad U_r(k) = \begin{bmatrix} u(k) \\ u(k+1) \\ \vdots \\ u(k+r-1) \end{bmatrix} \in R^{mr\times 1}, \text{ and} \tag{B3), (B4}$$

$$V_r(k) = \begin{bmatrix} v(k) \\ v(k+1) \\ \vdots \\ v(k+r-1) \end{bmatrix} \in R^{pr\times 1} \tag{B5}$$

Thus, Eq. (B2) is transformed as

$$Y_r(k) = \Gamma_r x(k) + S_r U_r(k) + V_r(k) \qquad (k = 1, 2, \ldots, N) \tag{B6}$$

where

$$\Gamma_r = \begin{bmatrix} C \\ CA \\ \vdots \\ CA^{r-1} \end{bmatrix} \in R^{pr\times n} \quad \text{and} \quad S_r = \begin{bmatrix} D & O^{p\times m} & \cdots & \cdots & O^{p\times m} \\ CB & D & O^{p\times m} & \cdots & \vdots \\ CAB & CB & D & \ddots & \vdots \\ \vdots & \vdots & \ddots & \ddots & O^{p\times m} \\ CA^{r-2}B & CA^{r-3}B & \cdots & CB & D \end{bmatrix} \in R^{pr\times mr} \tag{B7), (B8}$$

We define the matrices Y, U, X, and V as follows

$$Y = \begin{bmatrix} Y_r(1) & Y_r(2) & \cdots & Y_r(N) \end{bmatrix} \in R^{pr \times N}, \tag{B9}$$

$$U = \begin{bmatrix} U_r(1) & U_r(2) & \cdots & U_r(N) \end{bmatrix} \in R^{mr \times N}, \tag{B10}$$

$$X = \begin{bmatrix} x(1) & x(2) & \cdots & x(N) \end{bmatrix} \in R^{n \times N}, \text{ and} \tag{B11}$$

$$V = \begin{bmatrix} V_r(1) & V_r(2) & \cdots & V_r(N) \end{bmatrix} \in R^{pr \times N} \tag{B12}$$

Therefore, Eq. (B6) is transformed as

$$Y = \Gamma_r X + S_r U + V \tag{B13}$$

Here, the term $S_r U$ can be zero after whitening, and the noise term V can also be asymptotically zero with a suitable matrix Φ. Now, we consider a matrix G as an estimated value of Γ_r using input data $u(k)$. We pre- and post-multiply G by weighting matrices W_1 and W_2

$$\hat{G} = W_1 G W_2, \tag{B14}$$

and perform the singular value decomposition (SVD) of matrix $\hat{G}$ as follows

$$\hat{G} = U \Sigma V^T \approx U_s \Sigma_s V_s^T \tag{B15}$$

where U_s and V_s consist of the first n rows of U and V, respectively. $\Sigma_s \in R^{n \times n}$ is the upper-left part of Σ. We assume the system order n is unknown but the upper bound of system order n^* is known. We define the unknown full-rank matrix $\tilde{T} \in R^{n \times n^*}$

$$\hat{G} = \hat{\Gamma}_r \tilde{T} \tag{B16}$$

From Eqs. (B15) and (B16), we obtain

$$\hat{\Gamma}_r \tilde{T} V_s = U_s \Sigma_s \quad (\because V_s^T V_s = I) \quad \text{and} \quad \hat{\Gamma}_r = W_1^{-1} U_s R \tag{B17), (B18}$$

where R is an arbitrary matrix and typically $R = I$, $R = \Sigma_s$, or $R = \Sigma_s^{1/2}$ is chosen. The N4SID method adopts the following weighting matrices W_1 and W_2

$$W_1 = I \quad \text{and} \quad W_2 = \left(\frac{1}{N} \Phi \Pi_{U^T}^{\perp} \Phi^T \right)^{-1} \Phi \tag{B19), (B20}$$

where

$$\Pi_{U^T}^{\perp} = I - U^T (U U^T)^{-1} U \tag{B21}$$

The N4SID system identification procedure is summarized as follows:

1. Using input-output data, calculate matrix G with the following formula

$$G = \frac{1}{N} Y \Pi_{U^T}^{\perp} \Phi^T \tag{B22}$$

2. Choose weighting matrices W_1 and W_2, and perform SVD

$$\hat{G} = W_1 G W_2 = U \Sigma V^T \approx U_s \Sigma_s V_s^T \tag{B23}$$

3. Choose the full-rank matrix R, define the $pr \times n$ matrix $\hat{\Gamma}_r = W_1^{-1} U_s R$, and solve the following equations for $\hat{A}$ and $\hat{C}$

$$\hat{C} = \hat{\Gamma}_r(1:p, 1:n) \quad \text{and} \quad \hat{\Gamma}_r(p+1:pr, 1:n) = \hat{\Gamma}_r\left(1:p(r-1), 1:n\right)\hat{A} \tag{B24),(B25}$$

4. Estimate $\hat{B}$, $\hat{D}$, and the initial state variable $\hat{x}_0$ from the linear regression problem

$$\arg\min_{B,D,x_0} \frac{1}{N} \sum_{k=1}^{N} \left\| y(k) - \hat{C}(qI - \hat{A})^{-1} Bu(k) - Du(k) - \hat{C}(qI - \hat{A})^{-1} x_0 \delta(k) \right\|^2 \tag{B26}$$